Numerical Investigation of Natural Convection Within Horizontal Annulus with a Heated Protrusion

Shen-Min Liang*
National Cheng Kung University, Taiwan, Republic of China
and
Jyong-Jing Jiang†
Chung Shan Institute of Science and Technology, Taiwan, Republic of China

The objective of this paper is to investigate numerically the heat transfer phenomena associated with natural convection within a horizontal annulus with a heated element on the adiabatic inner cylinder. The Rayleigh number Ra based on the annulus gap is varied from 10^3 to 10^5, and the results were obtained with air as the working fluid. Stream function-vorticity formulation is used along with the Boussinesq approximation to model the laminar natural convection. The discretized energy and vorticity equations are solved by a two-step ADI technique. Numerical results show that the flow motion and heat transfer are greatly affected by the Rayleigh number and location of the heated element. When the heated element is at the bottom, tertiary flows set in for a Rayleigh number greater than about 5×10^4. The average Nusselt number is correlated by the relation $\overline{Nu} = C \cdot Ra^N$. Numerical results indicate that the constants C and N are functions of the inclination angle θ_h of the heated element.

Nomenclature

g = gravitational acceleration
L = gap of horizontal annulus
Nu = local Nusselt number defined by Eq. (19)
$\overline{Nu}$ = average Nusselt number defined by Eq. (20)
p = pressure
Pr = Prandtl number
R, r = dimensional and dimensionless coordinates, respectively
Ra = Rayleigh number based on L, $Ra = \rho g \beta L^3 (T_o - T_i)/\mu\alpha$
R_i, r_i = dimensional and dimensionless radii of inner cylinder, respectively
R_o, r_o = dimensional and dimensionless radii of outer cylinder, respectively
t = artificial time
T = dimensional temperature
T_i = dimensional temperature on heated element
T_o = dimensional temperature on outer cylinder
u_r, u = dimensional and dimensionless velocity components in radial direction, respectively
u_θ, v = dimensional and dimensionless velocity component in angular direction, respectively
α = thermal diffusivity of fluid
β = thermal volumetric expansion coefficient of fluid
θ = angular coordinate
θ_h = inclination angle of heated element
μ = viscosity of fluid
ρ = density of fluid
ϕ = dimensionless temperature
ψ = stream function
ω = vorticity

Presented as Paper 88-0658 at the AIAA 26th Aerospace Sciences Meeting, Reno, NV, Jan. 11-14, 1988; received Oct. 21, 1988; revision received March 13, 1989.

*Associate Professor, Institute of Aeronautics and Astronautics. Member AIAA.
†Assistant Scientist, Flight Control Division.

Introduction

NATURAL convection heat transfer in enclosures has been investigated over the last three decades due to engineering applications such as the cooling of electronic equipment, nuclear reactor design, solar systems, thermal storage, and underground electric power transmission. Natural convection in enclosures is characterized by convective cells due to the bouyancy effect, and heat transfer is represented by correlating the average Nusselt number as a function of the Rayleigh number, Prandtl number, and aspect ratio. Numerous papers on natural convection in enclosures have been published. Only a few will be mentioned here. We divide enclosure into two classes: cavity-type (simply connected) and annulus-type (multiply connected).

The flow phenomena of natural convection in a vertical slot have been studied by Elder[1] using flow visualization techniques. Chu et al.[2] further studied the effect of heater size, location, and aspect ratio on the laminar natural convection in rectangular channels. Chu et al. found that for a fixed Rayleigh number and heater size, there exists a maximum in average Nusselt number when the heater location is varied. The range of Rayleigh number is between 10^3 and 10^5. For higher Rayleigh numbers, natural convection in a rectangular channel was studied by Quon,[3] Küblbeck et al.,[4] and Fraikin et al.[5] More recently, problems of natural convection in enclosures with heated protrusions have drawn increased attention because the design of thermal control systems requires accurate heat transfer coefficient information. Jaluria[6] has numerically studied natural convection airflow due to multiple isolated heated elements. He found that the temperature and velocity fields depend on the heat input and distance between the heated elements. Kelleher et al.[7] experimentally investigated the laminar natural convection of water in a rectangular enclosure with a heated protrusion on one vertical wall, and Lee et al.[8] studied the problem numerically. Of particular interest is the finding that for a given Rayleigh number, the average Nusselt number decreases as the position of the heater is raised. Oosthuizen and Paul[9] further investigated the problem of a tilted square enclosure with a square heated element. The inclination angle of the tilted enclosure is varied from 0 to 90 deg. The numerical results of Oosthuizen and Paul show that the variation of the Nusselt number with the inclination

angle of the enclosure at a given Rayleigh number is not continuous. The reason for it was not explained.

According to the photographic results of Bishop and Carley,[10] the flow patterns in annulus-type enclosures can be classified into two basic patterns: the crescent pattern for small-diameter ratios and the kidney-shaped pattern for large-diameter ratios. Kuehn and Goldstein[11] further investigated the heat transfer of air and water in a horizontal cylindrical annulus using a combined theoretical and experimental approach. The Rayleigh number Ra based on the annulus gap was varied from 100 to 9.76×10^5. They found that the isotherms of air at $Ra = 1000$ are of the eccentric-circle shape and the flow is called a pseudoconductive regime. As the Rayleigh number is increased to 10^4, the buoyancy effect produces radial temperature inversion that indicates flow separation in the inner and outer cylinder. Kuehn and Goldstein also presented a correlation equation for the average Nusselt number, which is proportional to $Ra^{1/4}$. At a higher Rayleigh number, Jischke and Farshchi[12] found that the flow can be divided into five physically distinct regions: stagnant region, inner-boundary layer, outer-boundary layer, core, and thermal plume regions. Boyd[13] used the perturbation method to establish the correlation of the average Nusselt number as proportional to $Ra^{1/4}$ for steady natural convection heat transfer in horizontal annuli of an arbitrary cross section. When cylinders are not concentric, Prusa and Yao[14] found that the average Nusselt number is a convex function of the cylinder eccentricity. Instead of an isothermal inner cylinder, constant heat flux on the inner cylinder was considered by Van de Sande and Hamer[15] and Kumar.[16] Kumar's results show that the inner-wall temperature is strongly dependent on the diameter ratio. Axisymmetric natural convection between concentric spherical annuli has been studied by Astill et al.[17] and Masuoka et al.[18]

In the present paper, we consider natural convection in a horizontal cylindrical annulus with a heated element of finite size on the adiabatic inner cylinder. The study thus extends the previous studies on a horizontal cylindrical annulus that forms a special case of the present problem. The present problem arises in thermal control systems employed in aerospace vehicles. Although most practical situations involve three-dimensional flow, two dimensionality is assumed in the present study. In spite of this simplification, the present results should be helpful in analyzing the effect of heated-element position on convective motion and heat transfer. This problem was previously studied experimentally by Gau and Tang.[19] These authors found that the average Nusselt number is proportional to the one-third power of the Rayleigh number. However, the flow structure is not clearly shown due to limitation in the visualization technique. In the study of Gau and Tang, the Rayleigh number ranges from 10^6 to 10^8, which is in the regime of turbulent flow.[20] For steady laminar flows, the average Nusselt number may not be proportional to the one-third or one-fourth power of Rayleigh number. The exponent may be a function of the heated-element location. Thus, the objective of the present study is to establish the correlation between the average Nusselt number and Rayleigh number, and to investigate the detailed flow motion, temperature field, and the effect of heated-element location. The Rayleigh number chosen ranges from 10^3 to 10^5, which is in the regime of laminar convection.

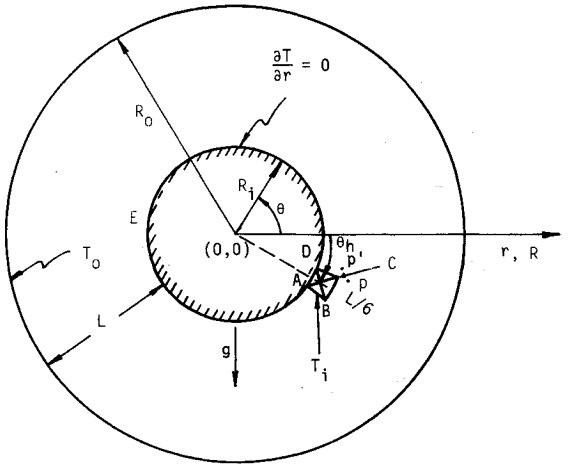

Fig. 1 A sketch of physical problem.

Physical Problem and Mathematical Model

Consider a fluid inside a horizontal cylindrical annulus under the gravitational field. The temperature on the outer cylinder is maintained at T_o. The inner cylinder is adiabatic. On the inner cylinder there is a heated element of finite shape and size. The heated-element shape is assumed to be almost a square with side $L/6$ and is inclined at an angle θ_h. On the heated element the temperature is assumed to be T_i, which is greater than T_o. The physical problem is sketched in Fig. 1.

Assume that the flow dimensional, laminar, and steady, and that there is no viscous dissipation. The governing equations are the Navier-Stokes and energy equations. If we use the Boussinesq approximation, which assumes that fluid properties are constant except for density in the momentum equations, the continuity, momentum, and energy equations in cylindrical coordinates (R, θ) become

$$\frac{\partial u_r}{\partial R} + \frac{u_r}{R} + \frac{1}{R}\frac{\partial u_\theta}{\partial \theta} = 0 \tag{1}$$

$$\rho\left(u_r \frac{\partial u_r}{\partial R} + \frac{u_\theta}{R}\frac{\partial u_r}{\partial \theta} - \frac{u_\theta^2}{R}\right) = -\frac{\partial p}{\partial R} + \mu\left(\frac{\partial^2 u_r}{\partial R^2} + \frac{1}{R}\frac{\partial u_r}{\partial R} + \frac{1}{R^2}\frac{\partial^2 u_r}{\partial \theta^2} - \frac{u_r}{R^2} - \frac{2}{R^2}\frac{\partial u_\theta}{\partial \theta}\right) + \rho g \beta (T - T_o)\cos\theta \tag{2}$$

$$\rho\left(u_r \frac{\partial u_\theta}{\partial R} + \frac{v_\theta}{R}\frac{\partial u_\theta}{\partial \theta} + \frac{u_r u_\theta}{R}\right) = -\frac{1}{R}\frac{\partial p}{\partial \theta} + \mu\left(\frac{\partial^2 u_\theta}{\partial R^2} + \frac{1}{R}\frac{\partial u_\theta}{\partial R} + \frac{1}{R^2}\frac{\partial^2 u_\theta}{\partial \theta^2} - \frac{u_\theta}{R^2} + \frac{2}{R^2}\frac{\partial u_r}{\partial \theta}\right) + \rho g \beta (T - T_o)\sin\theta \tag{3}$$

$$u_r \frac{\partial T}{\partial R} + \frac{u_\theta}{R}\frac{\partial T}{\partial \theta} = \alpha\left(\frac{\partial^2 T}{\partial R^2} + \frac{1}{R}\frac{\partial T}{\partial R} + \frac{1}{R^2}\frac{\partial^2 T}{\partial \theta^2}\right) \tag{4}$$

Introduce dimensionless variables

$$r = \frac{R}{L}, \quad \phi = \frac{T - T_o}{T_i - T_o}, \quad u = \frac{u_r L}{\alpha}, \quad v = \frac{v_\theta L}{\alpha} \tag{5}$$

and the stream function ψ and vorticity ω by setting

$$u = \frac{1}{r}\frac{\partial \psi}{\partial \theta}, \qquad v = -\frac{\partial \psi}{\partial r} \tag{6}$$

$$\omega = -\left(\frac{\partial^2 \psi}{\partial r^2} + \frac{1}{r}\frac{\partial \psi}{\partial r} + \frac{1}{r^2}\frac{\partial^2 \psi}{\partial \theta^2}\right) \tag{7}$$

The stream function automatically satisfies the continuity equation (1). After the introduction of dimensionless variables and the stream function-vorticity (ψ, ω), the Navier-Stokes equations (1-4) lead to the Poisson equation and energy and vorticity transport equations

$$\frac{\partial^2 \psi}{\partial r^2} + \frac{1}{r}\frac{\partial \psi}{\partial r} + \frac{1}{r^2}\frac{\partial^2 \psi}{\partial \theta^2} = -\omega \tag{8}$$

$$u\frac{\partial \phi}{\partial r} + \frac{v}{r}\frac{\partial \phi}{\partial \theta} = \frac{\partial^2 \phi}{\partial r^2} + \frac{1}{r}\frac{\partial \phi}{\partial r} + \frac{1}{r^2}\frac{\partial^2 \phi}{\partial \theta^2} \tag{9}$$

$$u\frac{\partial\omega}{\partial r}+\frac{v}{r}\frac{\partial\omega}{\partial\theta}=Pr\left(\frac{\partial^2\omega}{\partial r^2}+\frac{1}{r}\frac{\partial\omega}{\partial r}+\frac{1}{r^2}\frac{\partial^2\omega}{\partial\theta^2}\right)+RaPr\left(\cos\theta\frac{\partial\phi}{\partial r}-\frac{1}{r}\sin\theta\frac{\partial\phi}{\partial\theta}\right) \quad (10)$$

Numerical Method

Finite-Difference Approximation

Equations (8–10) are solved by the finite-difference approximation. Central-difference formulas are used for all spatial derivative terms, convective terms included, in the Poisson, energy, and vorticity equations. The Poisson equation and transport equations are modified by adding a false-transient term to them. For example, the term $\partial\psi/\partial t$ is added to Eq. (8). The time derivatives are discretized by first-order backward differencing. The two-step alternating direction implicit (ADI) method is used to solve the discretized equations by inverting tridiagonal matrices.

Boundary Conditions

Since the velocity vanishes at the outer and inner walls, the stream function at the walls is set to zero. Thus, we have at the outer wall

$$\psi=u=v=0,\quad \phi=0,\quad \omega=-\frac{\partial^2\psi}{\partial r^2}\quad \text{at}\quad r=r_o \quad (11)$$

and at the inner wall

$$\psi=u=v=0 \quad (12)$$

$$\frac{\partial\phi}{\partial r}=0\qquad \text{for adiabatic portion } AED \quad (13)$$

$$\phi=1\qquad \text{for isothermal portion } ABCD \quad (14)$$

$$\omega=\begin{cases}-\partial^2\psi/\partial r^2 & \text{on side } BC\\ -\partial^2\psi/r^2\partial\theta^2 & \text{on sides } AB \text{ and } CD\end{cases} \quad (15)$$

as shown in Fig. 1. Here, letters A, B, and C, D denote the corners of the heated element. One-sided difference formulas are used for the Neumann boundary conditions to enhance numerical stability.[4] Since vorticity is singular at points B and C, multiple-valued vorticity is defined at these two points. For example, at point C, the vorticity is defined as either

$$\omega=-\frac{2\psi_p}{\Delta r^2} \quad (16)$$

or

$$\omega=-\frac{2\psi_{p'}}{r^2\Delta\theta^2} \quad (17)$$

depending on the sweeping direction, where points p and p' are two nodal points close to point C (see Fig. 1).

Solution Procedure

The solution procedure used to obtain the steady-state solution is described as follows:

1) Specify the initial guess for the temperature, vorticity, and stream function.

2) Solve the energy and vorticity equations at $n+\frac{1}{2}$ time step.

3) Solve the Poisson equation for the stream function at $n+\frac{1}{2}$ time step.

4) Repeat steps (2) and (3) at $n+1$ time step.

5) Compute velocity field in the solution domain and vorticity at the boundaries.

6) Check for convergence by the criterion

$$|f_{i,j}^{n+1}-f_{i,j}^{n}|<\epsilon,\qquad f=\phi,\ \omega,\ \psi \quad (18)$$

for all i, j, where ϵ is a preassigned value. The procedure is repeated until the convergence condition Eq. (18) is satisfied.

Results and Discussion

All numerical calculations were performed on a VAX8600 computer. A uniform grid with 37×152 grid points was used. In order to ensure the accuracy of numerical solutions, a finer grid with half the grid size of the coarse grid was tested. It was found that the computed average Nusselt number at $\theta_h=-90$ deg and $Ra=50{,}000$ is 0.728 on the coarse grid, 0.733 on the fine grid, and 0.738 for the Richardson extrapolation. This shows that the improvement of the fine-grid solution is not significant (about 0.7%) and that the coarse-grid solution is reasonably accurate. The preassigned value ϵ was chosen as 1×10^{-4}.

To verify the program developed, the problem of natural convection heat transfer between two isothermal horizontal cylinders was solved for $Ra=5\times10^4$ and $Pr=0.7$. The computed temperature distributions were compared with the experimental data of Kuehn and Goldstein under the same conditions ($R_o/R_i=2.6$). Both results are in good agreement.

The results reported here were obtained for air ($Pr=0.7$). The Rayleigh number ranged from 1×10^3 to 1×10^5. The ratio of R_o to R_i was chosen to be 3. Qualitatively similar results exist for different-diameter ratios. The effect of the heated-element position on the steady flow motion and heat transfer rate at different Rayleigh numbers was studied. Following accepted practice, we let Nu be the local Nusselt number, defined as

$$Nu=-\ell n\left(\frac{r_o}{r_i}\right)r\frac{\partial\phi}{\partial r} \quad (19)$$

and $\overline{Nu}$ be the average Nusselt number at the outer cylinder; namely,

$$\overline{Nu}=-\frac{r_o}{2\pi}\ell n\left(\frac{r_o}{r_i}\right)\int_0^{2\pi}\left.\frac{\partial\phi}{\partial r}\right|_{r=r_o}d\theta \quad (20)$$

The correlations between the average Nusselt number and Rayleigh number at different heated-element locations are established. Five cases were considered: $\theta_h=-90$ deg, -45 deg, 0 deg, 45 deg, and 90 deg. Only three cases, $\theta_h=-90$ deg, 0 deg, and 90 deg, are reported in this paper. The flow motion and isotherms for the cases of -45 and 45 deg reported in Ref. 21 are qualitatively similar to those of the foregoing three cases.

Flow Structures and Isotherms

First, we study the effect of the Rayleigh number on the flow motion and temperature field.

Case 1, $\theta_h=-90$ deg

In this case the heated element is located at the bottom. The fluid heated by the heated element changes its density and hence produces a buoyancy force that drives the heated fluid upward. Because the top fluid is cooler, the ascending fluid, transferring its heat to the adjacent cooler fluid, is cooled down and encounters an adverse pressure gradient. The adverse pressure gradient forces the ascending fluid to separate from the adiabatic wall. The separated fluid forms a thermal plume that impinges on the outer cylinder. After the impingement, the fluid being cooled by the outer wall descends toward the bottom of the annulus. Hence, steady recirculating flows, called primary convection cells, are formed on both sides because of the symmetry of heating. Induced by the primary convection cells, two additional cells are developed at the

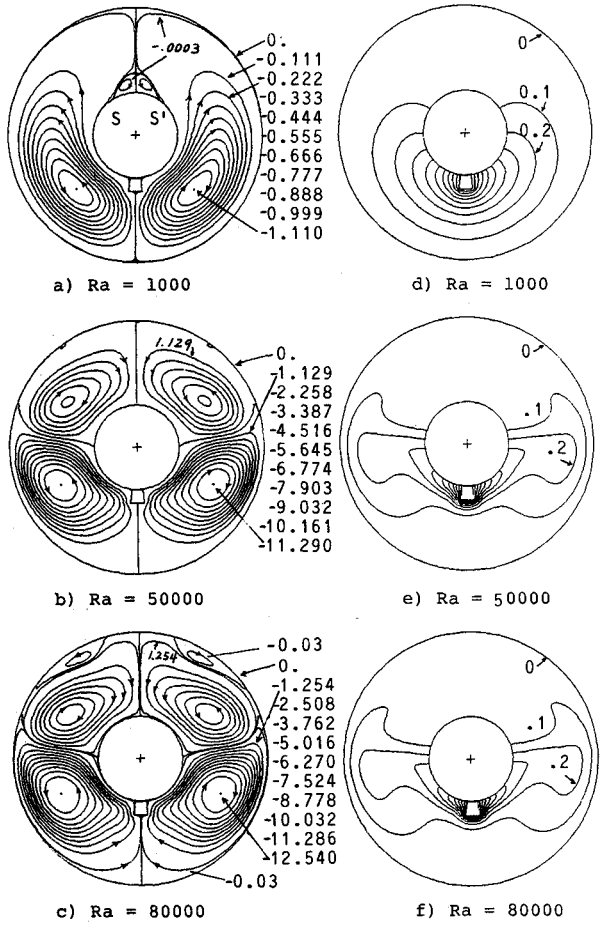

Fig. 2 Streamlines and isotherms for different Rayleigh numbers when $\theta_h = -90$ deg. a) $Ra = 1000$; b) $Ra = 50{,}000$; c) $Ra = 80{,}000$; d) $Ra = 1000$; e) $Ra = 50{,}000$; f) $Ra = 80{,}000$.

top due to the viscous forces. At a low Rayleigh number ($Ra \leq 1000$), the flow speed is slow and the heat transfer is mainly due to conduction. Thus, the temperature field is close to the solution of the Laplace equation, $\nabla^2\phi = 0$ (see Figs. 2d and 4d). Figure 2a shows the symmetric circulating cells denoted by streamlines when $Ra = 1000$. The induced cells are very small and form an almost stagnant region. The inner-cylinder boundary layers separate at points S and S', which are inclined about 30 deg from the vertical. The rotation centers of the primary cells lie on the $\theta = 48$ deg (acute angle) line from the vertical. The corresponding temperature field is shown in Fig. 2d. The isotherms have a heart-like shape.

As the Rayleigh number increases, the primary and induced cells grow in physical extent. Thus, the induced cells grow and occupy more space, the primary cells rotate faster, but shrink in size. Figure 2b shows the primary and induced recirculating cells when $Ra = 5 \times 10^4$. It is seen that the size of the induced cells is comparable to the primary cells. Note that there are two other induced convection cells, called the tertiary flow, which develop at the outer cylinder. Thus, the tertiary flow sets in for a Rayleigh number approximately greater than 5×10^4. Figure 2e shows the corresponding temperature field. Because of the strong convection effect, the isotherms are distorted as compared with Figure 2d, and multiple inflexion points are present. These inflexion points correspond to the separation of the inner- and outer-cylinder thermal boundary layers.

As the Rayleigh number is further increased, the flow pattern and temperature field do not change significantly, except that the tertiary flow grows in intensity. However, the tertiary flows have no effect on the overall heat transfer. Figures 2c and 2f show the flow motion and corresponding temperature

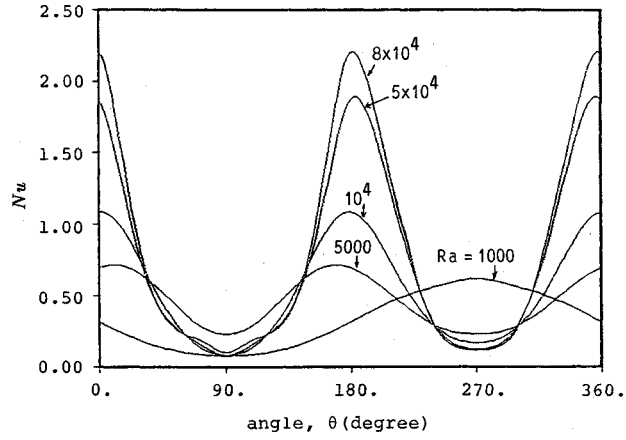

Fig. 3 The distributions of the local Nusselt number on the outer cylinder when $\theta_h = -90$ deg.

distribution when $Ra = 80{,}000$. One can clearly see the tertiary flows at the top in Fig. 2c. The isotherms in Fig. 2f are similar to those in Fig. 2e, except for further distortion.

The local heat transfer on the outer cylinder is of interest to engineers. Figure 3 shows the distribution of the local Nusselt number at the outer cylinder for different Rayleigh numbers. When $Ra = 1000$, there is only one peak at $\theta = 270$ deg and one trough at $\theta = 90$ deg, since the heat transfer is close to pure conduction. As the Rayleigh number increases, convection is more effective and the peak becomes a trough. Because of the thermal plumes that develop near $\theta = 0$ deg and $\theta = 180$ deg (the horizontal coordinate in Fig. 1), there are two peaks near the horizontal axis for the higher Rayleigh number case.

Case 2, $\theta_h = 0$ deg

When the heated element is located on the horizontal axis, the primary convection cell forms at the right-hand side and induces different flow motions at the left-hand side, depending on the Rayleigh number. At $Ra = 1000$, the induced cellular circulation consists of two smaller cells with the same rotating direction (counterclockwise). These two cells produce a stagnation region near the 9 o'clock position of the annulus, as shown in Fig. 4a. Note that the primary cell has negative values of stream function and the induced cells have positive values. Since the heat transfer is not purely conductive, the isotherms shown in Fig. 4d are not completely symmetric with respect to the horizontal axis. As the Rayleigh number increases, the maximum values of the stream function are increased, which indicates that the circulation speed of the convection cells is intensified. This leads to the merging of the induced convection cells. Moreover, the primary cell shrinks in size, and the thermal plume moves downward. Figure 4b shows the primary and induced cells when $Ra = 50{,}000$. As implied by the maximum stream functions, one can see that the rotation intensities of these two cells are comparable. Figure 4e shows the corresponding isotherms that are highly distorted. As the Rayleigh number is increased to 10^5, the patterns of the flow and temperature fields do not change significantly, as shown in Figs. 4c and 4f. The variations of the local Nusselt number at the outer cylinder at different Rayleigh numbers are shown in Fig. 5. This figure shows that the maximum heat transfer rate occurs at about $\theta = 17$ deg. Away from the peak, the local Nusselt number is almost zero.

Case 3, $\theta_h = 90$ deg

When the heated element is on top, the flow pattern (Figs. 6a–6b) is just the reverse of that shown in Fig. 2a. In this case, the primary circulating cells are on the top and the induced cells are right below the inner cylinder and form a dead region. As the Rayleigh number increases, the induced cells grow slowly. The isotherms change from circular- to mushroom-

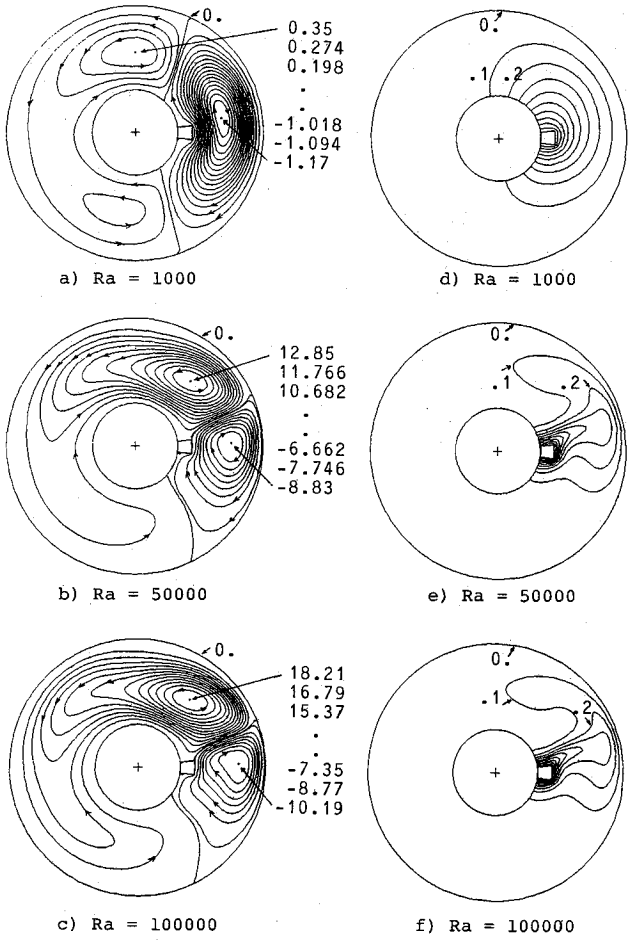

Fig. 4 Streamlines and isotherms for different Rayleigh numbers when $\theta_h = 0$ deg. a) $Ra = 1000$; b) $Ra = 50{,}000$; c) $Ra = 100{,}000$; d) $Ra = 1000$; e) $Ra = 50{,}000$; f) $Ra = 100{,}000$.

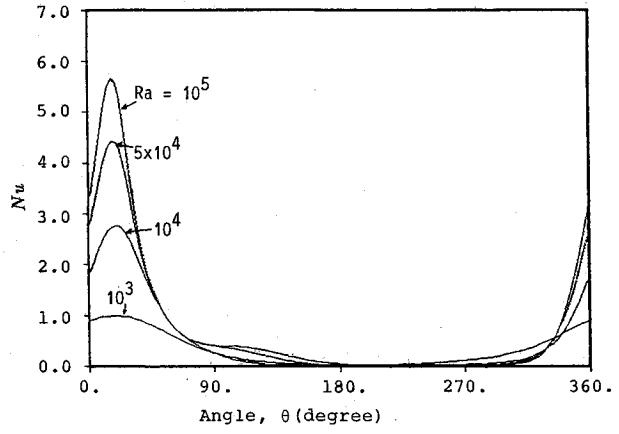

Fig. 5 The distributions of the local Nusselt number on the outer cylinder when $\theta_h = 0$ deg.

shaped, as shown in Figs. 6c–6d. Because the thermal plume lies on the vertical line, the local Nusselt number attains its maximum value at $\theta = 90$ deg, the location of the stagnation point.

Effect of Heater Location

Next, we study the effect of the heated-element location on the local heat transfer rate. We fix the Rayleigh number by letting $Ra = 50{,}000$. Qualitatively similar results can be obtained for other values of Ra. The variations of the local Nusselt number at the outer cylinder for different heated-element locations are plotted in Fig. 7. It is shown that the

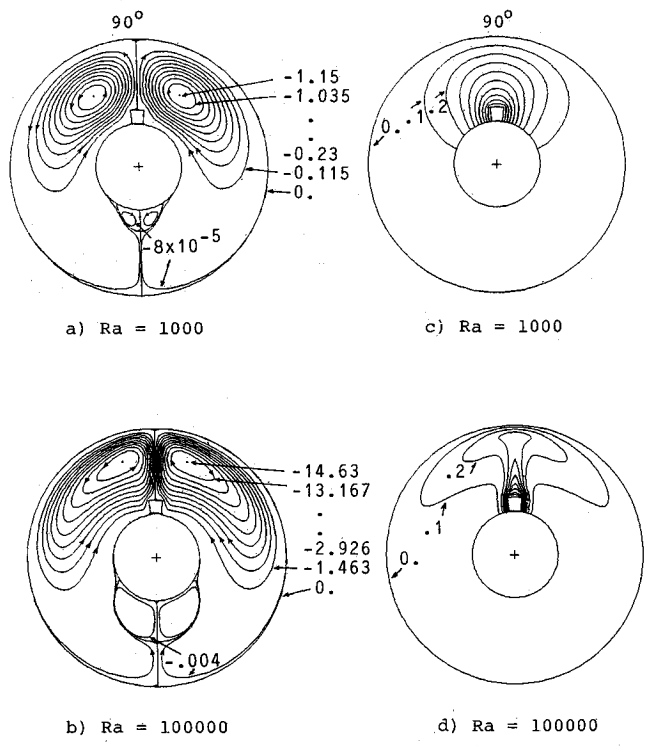

Fig. 6 Streamlines and isotherms for two Rayleigh numbers when $\theta_h = 90$ deg. a) $Ra = 1000$; b) $Ra = 100{,}000$; c) $Ra = 1000$; d) $Ra = 100{,}000$.

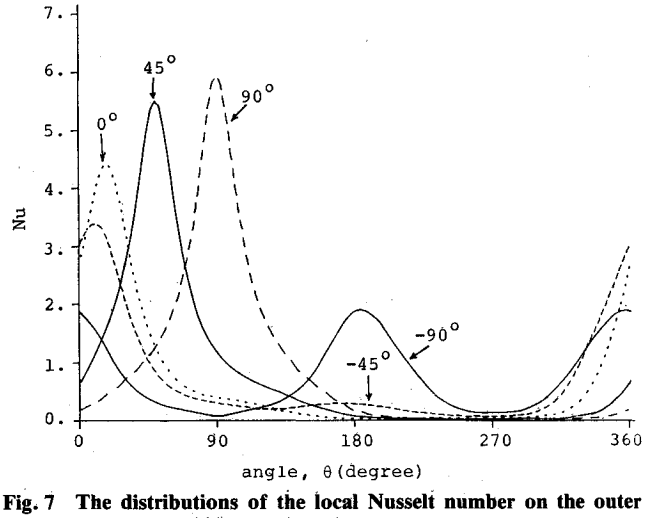

Fig. 7 The distributions of the local Nusselt number on the outer cylinder at $Ra = 50{,}000$ at various θ_h.

peak location moves from $\theta = 0$ deg to $\theta = 90$ deg, as the heated-element position is changed from the bottom to the top. Because of the effect of both convection and conduction, the maximum value increases with θ_h.

The average Nusselt number Nu has been computed and plotted vs the heated-element location θ_h. Figure 8 shows that there exists a minimum in the average Nusselt number when $\theta_h = -11$ deg and that an abrupt change in Nu occurs when θ_h is changed from -18 to -11 deg. The abrupt decrease in Nu is due to the flow blockage caused by the heating element. The blockage slows down the convection speed of the primary cell and reduces the heat transfer rate. To confirm this point, we reduced the height of the heated element by a factor of 2. In this case, it was found that the minimum disappeared.

Finally, the correlation between the average Nusselt number and the Rayleigh number through the relation $Nu = C(\theta_h)\, Ra^{N(\theta_h)}$ is established at different heated-element positions, where the parameters $C(\theta_h)$ and $N(\theta_h)$ are functions of θ_h to be

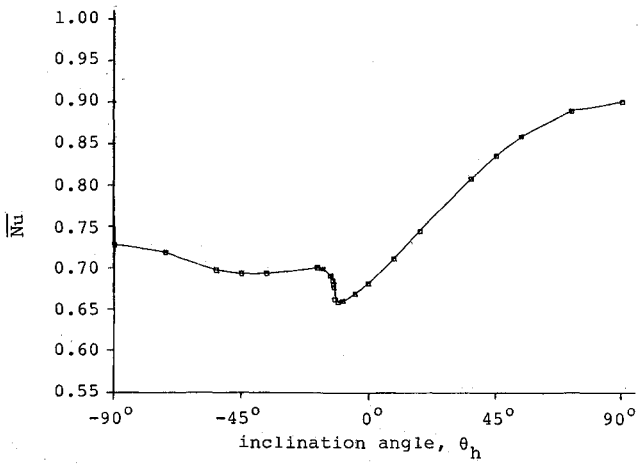

Fig. 8 The effect of the heated-element position on the average Nusselt number $\overline{Nu}$ at $Ra = 50{,}000$.

Table 1 Computed values for constants C and N in the Correlation $\overline{Nu} = C\,Ra^N$

θ_h, deg	Number of data used	Constant, C	Power, N
−90	8	0.0798	0.205
−45	8	0.0872	0.192
0	11	0.0841	0.195
45	8	0.0631	0.238
90	10	0.0593	0.251

determined. Table 1 gives the computed values of $C(\theta_h)$ and $N(\theta_h)$ for different values of θ_h. In Table 1 the number of data points used to obtain the constants C and N are indicated. When $\theta_h = 45$ deg, N has the largest value of 0.192. When $\theta_h = 90$ deg, N has the largest value of 0.251, which is close to 0.25, valid for the case of two isothermal horizontal cylinders.

Conclusions

Natural convection heat transfer within the annulus of two horizontal concentric cylinders with a heated element on the adiabatic inner cylinder has been studied. The effect of the heated-element position at different Rayleigh numbers on the flow motion and heat transfer rate is investigated. When the heated element is located at the bottom, a tertiary flow sets in for a Rayleigh number greater then approximately 5×10^4.

The correlation between the average Nusselt number and Rayleigh number has been established. The constants $C(\theta_h)$ and $N(\theta_h)$ in the correlation, $\overline{Nu} = C(\theta_h)Ra^{N(\theta_h)}$, are computed for different heated-element locations. There exists a minimum value in the average Nusselt number when θ_h is varied. When $Ra = 5 \times 10^4$, it is found that the minimum value is equal to 0.66 at $\theta = -11$ deg, and an abrupt decrease in $\overline{Nu}$ occurs as θ_h is changed from -18 to -11 deg. The abrupt change is due to the blockage of the heated element on the ascending heated fluid.

Acknowledgments

The authors are grateful to Professors W. Aung and L. S. Yao for their helpful comments and to Dr. C. Gau for valuable discussions during the preparation of this paper. The authors wish to express their appreciation to the Institute of Aeronautics and Astronautics, National Cheng Kung University, for providing computer time. This study was sponsored by the National Science Council, China.

References

[1]Elder, J. W., "Turbulent Free Convection in a Vertical Slot," *Journal of Fluid Mechanics,* Vol. 23, Part 1, 1965, pp. 99–111.

[2]Chu, H. H.-S., Churchill, S. W., and Patterson, C. V. S., "The Effect of Heater Size, Location, Aspect Ratio, and Boundary Condition in Rectangular Channels," *Journal of Heat Transfer,* Vol. 98, Ser. C, No. 2, 1976, pp. 194–201.

[3]Quan, C., "High Rayleigh Number Convection in an Enclosure—A Numerical Study," *The Physics of Fluids,* Vol. 15, No. 1, 1972, pp. 12–19.

[4]Küblbeck, K., Merker, G. P., and Straub. J., "Advanced Numerical Computation of Two-Dimensional Time-Dependent Free Convection in Cavities," *International Journal of Heat and Mass Transfer,* Vol. 23, No. 2, 1980, pp. 203–216.

[5]Fraikin, M. P., Portier, J. J., and Fraikin, C. J., "Application of a $k-\epsilon$ Turbulence Model to an Enclosure Buoyancy Driven Recirculating Flow," American Society of Mechanical Engineers, ASME Paper 80-HT-68, July 27–30, 1980.

[6]Jaluria, Y., "Buoyancy-Induced Flow due to Isolated Thermal Sources on a Vertical Surface," *Journal of Heat Transfer,* Vol. 104, No. 2, 1982, pp. 223–227.

[7]Kelleher, M. D., Knock, R. H., and Yang, K. T., "Laminar Natural Convection in a Rectangular Enclosure Due to a Heated Protrusion on One Vertical Wall—Part I: Experimental Investigation," *Proceedings of the 1987 ASME/JSME Thermal Engineering Joint Conference,* Vol. 2, pp. 169–179.

[8]Lee, J. J., Liu, K. V., Yang, K. T., and Kelleher, M. D., "Laminar Natural Convection in a Rectangular Enclosure Due to a Heated Protrusion on One Vertical Wall—Part II: Numerical Simulations," *Proceedings of the 1987 ASME/JSME Thermal Engineering Joint Conference,* Vol. 2, pp. 179–185.

[9]Oosthuizen, P. H. and Paul, J. T., "Effect of Cap Shape on Free Convection Heat Transfer Across a Cavity," *Proceedings of the 1987 ASME/JSME Thermal Engineering Joint Conference,* Vol. 2, pp. 221–226.

[10]Bishop, E. H. and Larley, C. T., "Photographic Studies of Natural Convection Between Concentric Cylinders," *Proceedings of the 1966 Heat Transfer and Fluid Mechanics Institute,* Stanford University Press, Stanford, CA, 1966 pp. 63–78.

[11]Kuehn, T. H. and Goldstein R. J., "An Experimental and Theoretical Study of National Convection in the Annulus Between Horizontal Concentric Cylinders," *Journal of Fluid Mechanics,* Vol. 74, Part 4, 1976, pp. 695–714.

[12]Jischke, M. C. and Farshchi, M., "Boundary-Layer Regime for Laminar Free Convection Between Horizontal Circular Cylinders," *Journal of Heat Transfer,* Vol. 102, No. 2, May 1980, pp. 228–235.

[13]Boyd, R. D., "A Correlation Theory for Steady Natural Convection Heat Transport in Horizontal Annuli," *Journal of Heat Transfer,* Vol. 105, No. 1, Feb. 1983, pp. 144–150.

[14]Prusa, J. and Yao, L. S., "Natural Convection Heat Transfer Between Eccentric Horizontal Cylinders," *Journal of Heat Transfer,* Vol. 105, No. 1, Feb. 1983, pp. 108–116.

[15]Van de Sande, E. and Hamer, B. J. G., "Steady Transient Natural Convection in Enclosure Between Horizontal Circular Cylinders (Constant Heat Flux)," *International Journal of Heat and Mass Transfer,* Vol. 22, Feb. 1979, pp. 361–370.

[16]Kumar, R., "Numerical Study of Natural Convection in a Horizontal Annulus With Constant Heat Flux on the Inner Wall," *Proceedings of the 1987 ASME/JSME Thermal Engineering Joint Conference,* Vol. 2, pp. 187–193.

[17]Astill, K. N., Leong, H., and Martorana, R., "A Numerical Solution for Natural Convection in Concentric Spherical Annuli," paper presented at the *19th National Heat Transfer Conference,* ASME HTD, Vol. 8, 1980, pp. 105–113.

[18]Masuoka, T., Ishizaka, K., and Katsuhara, T., "Heat Transfer by Natural Convection in Porous Media Between Two Concentric Spheres," American Society of Mechanical Engineers, ASME HTD, Vol. 8, 1980, pp. 115–120.

[19]Gau, C. and Tang, U. H., "Experimental Studies of Natural Convection Heat Transfer Within Horizontal Annulus with a Heating Element on Inner Cylinder," AIAA/ASME Paper 86-HT-8, 1986.

[20]Farouk, B. and Güçeri, S. I., "Laminar and Turbulent Natural Convection in the Annulus Between Horizontal Concentric Cylinders," *Journal of Heat Transfer,* Vol. 104, No. 4, Nov. 1982, pp. 631–636.

[21]Liang, S. M. and Jiang, J. J., "A Numerical Investigation of Natural Convection Heat Transfer Within a Horizontal Annulus with a Heating Element on the Inner Cylinder," AIAA Paper 88-0658, Jan. 1988.